# Grid independence behaviour of fluidized bed reactor simulations using the Two Fluid Model: Effect of particle size

*Schalk Cloete[1], Stein Tore Johansen[2] & Shahriar Amini[2*]*

[1] NTNU Department of Energy and Process technology, Trondheim, NORWAY

[2] SINTEF Materials and Chemistry, Trondheim, NORWAY

*Corresponding author:

Dr. Shahriar Amini

Department of Process Technology

SINTEF Materials and Chemistry

Richard Birkelands Vei 3

7034 Trondheim, Norway

Phone: +47 46639721

Email: shahriar.amini@sintef.no

# 1 Abstract

It is well known that particle size has a significant influence on the grid independence behaviour of fluidized bed reactor simulations carried out using the Two Fluid Model (TFM) approach. The general rule of thumb states that the cell size should scale linearly with the particle size so that the cell size is always at most a factor of 10 larger than the particle size. In this study, however, the effect of particle size on grid independence behaviour was shown to be unexpectedly large. In particular, a five-fold increase in particle size permitted the use of a 63 times larger cell size, implying a $63^3 \approx 250{,}000$ times speedup for resolved simulations in the planar 2D domain considered in this study. Thus, the general rule of thumb was found to be overly cautious, especially for larger particles. Closer investigation revealed the particle relaxation time to be a very good predictor of the grid independent cell size. Although this finding needs to be confirmed for parameters other than only the particle size, this relation can theoretically be used to greatly shorten the time-consuming grid independence studies that are required before any fluidized bed simulation campaign. In general, the rapid increase in cell size allowed by larger particle sizes showed that reasonably accurate industrial scale simulations (5 m inner diameter reactor) are already possible in 2D for large particles (~600 μm). If the 2D grid independence behaviour assessed in this study is extendible to 3D, larger particle sizes in the range of 500-1000 μm can already be simulated in full 3D for reactor sizes ranging from 1-4 m. Simulation of smaller particle sizes (<200 μm) will remain out of reach for many decades to come, however, and a filtered coarse grid approach will definitely be required to make such simulations possible.

# 2 Introduction

Fluidized bed reactors are widely used in the process industry for applications involving gas-solid reactions or solid catalysed reactions. The excellent heat and mass transfer characteristics of these reactors are highly advantageous from a process engineering point of view and it can therefore be assumed that the number of process applications utilising this technology will only increase in the future.

Fluidized bed reactors are challenging to design and scale up, however, primarily due to the complex transient process nature created by the formation of mesoscale particle structures inside the bed. These particle structures are observed as clusters in risers and bubbles in bubbling fluidized beds and result from the non-linear drag interaction between the gas and the solids. When designing a fluidized bed reactor, these structures cannot be ignored because they have a profound influence on all transport phenomena inside the reactor.

This complex hydrodynamic behaviour of fluidized bed reactors is closely coupled to reaction kinetics and heat transfer considerations. For example, the formation of the structures has a negative influence on the overall reaction rate by concentrating particles (and therefore surface area for reaction) in dense clusters that have a low gas permeability [1]. The result is a severe mass transfer limitation because reacting gases cannot penetrate fast enough into the cluster. Thus, if this cluster effect is not accurately accounted for in reactor design and scale up considerations, reactor performance will be greatly over-predicted, leading to misleading design guidelines.

In this work, the fundamental modelling framework of computational fluid dynamics (CFD) is proposed as a suitable modelling tool. Because of its fundamental basis in the conservation of mass, momentum, species and energy, CFD is capable of inherently capturing the complex

mesoscale structure formation and the resulting non-linear interactions that make fluidized bed reactors a difficult modelling challenge.

CFD approaches for modelling fluidized bed reactors have been developed to a good level of maturity over the past three decades, primarily based on the kinetic theory of granular flows (KTGF) [2-4] where the random uncorrelated motions of particles are likened to the motions of molecules in a gas. This approach has been used extensively in the literature and some favourable hydrodynamic validation studies have also been performed [5-7]. However, the primary limitation of these methods is the fine spatial and temporal resolution required to accurately resolve the mesoscale structures. Thus, simulations of industrial scale fluidized bed reactors are not computationally affordable for the majority of cases.

The most promising approach for meeting this challenge is to model the effects of these mesoscale structures on grid sizes that can be larger than the structure itself. An increasing body of literature focusing on the subject is already available (e.g. [8-11]). However, the additional modelling included in this filtered approach introduces a substantial degree of uncertainty simply due to the complex nature of the subgrid clustering phenomena. After more than a decade of development, current closures for the drag and solids stresses appear to function reasonably well with uncertainties still present in areas with large flow gradients such as near-wall regions [12]. A first closure for first order heterogeneous reactions has recently been proposed [13] and heat transfer correlations are yet to be developed.

Therefore, this work strives to find the real limits of an approach which is mature already today: the TFM/KTGF approach. It is well known that the grid independence behaviour of TFM simulations is strongly correlated with the particle size simulated. In general, fluidized beds using larger particle sizes can be simulated on coarser grids with cell sizes often specified at 10 times the particle size as a general rule of thumb. With the consistent exponential increase in

computational capacity and availability, it can therefore be reasoned that the particle size that can be directly simulated in an industrial scale fluidized bed will gradually decrease with time. Some guidelines can be found in this work regarding the size of fluidized bed that can be directly simulated with existing models and a specified particle size using computational capacities available today.

# 3 Nomenclature

Main Symbol definitions:

$\alpha$ Volume fraction

$\Delta_{lin}$ Linearized grid size

$\phi$ Kinetic energy transfer rate ($W/m^3$)

$\gamma$ Dissipation rate ($W/m^3$)

$\Theta_s$ Granular temperature ($m^2/s^2$)

$\mu$ Viscosity (Pa.s)

$\rho$ Density ($kg/m^3$)

$\varsigma$ Specularity coefficient

$\bar{\bar{\tau}}$ Stress tensor (Pa)

$\vec{\tau}_s$ Particle shear force at the wall (N)

$\tau_s$ Particle relaxation time (s)

$\tau_{s_S}$ Stokes relaxation time (s)

$\vec{v}$ Velocity vector (m/s)

$\nabla$ Del operator / Gradient (1/m)

Ar Archimedes number

$C$ Molar concentration (mol/m$^3$)

$C_D$ Drag coefficient

$d$ Diameter (m)

$\vec{g}$ Gravity vector (m/s$^2$)

$g_{0,ss}$ Radial distribution function

$\bar{\bar{I}}$ Identity tensor

$\vec{J}$ Diffusive flux (kg/(m$^2$.s))

$K$ Momentum exchange coefficient (kg/(m$^3$.s))

$k$ Reaction rate constant (m/s)

$k_{\Theta_s}$ Granular temperature diffusion coefficient (kg/(m.s))

$M$ Molar mass (kg/mol)

$N$ Moles (mol)

$p$ Pressure (Pa)

$R$ Gas constant (8.314 J/(K.mol))

| | |
|---|---|
| Re | Reynolds number |
| $R_H$ | Heterogeneous reaction rate (mol/(m$^3$s)) |
| $S$ | Source term (kg/m$^3$s) |
| $T$ | Temperature (K) |
| $t$ | Time (s) |
| $U$ | Fluidization velocity (m/s) |
| $\vec{U}_{s,\parallel}$ | Particle velocity parallel to wall (m/s) |
| $V$ | Volume (m$^3$) |
| $X$ | Reactor performance parameter |
| $Y$ | Mass fraction |

Sub- and superscript definitions:

| | |
|---|---|
| $A$ | Species A |
| $g$ | Gas |
| $gs$ | Interphase |
| $i$ | Species index |
| $n$ | Reaction order |
| $s$ | Solids |

# 4 Simulations

## 4.1 Model equations

The equation system for the well-known TFM KTGF approach will be briefly outlined below. This approach has been confirmed to give adequate representations of the hydrodynamics of fluidized bed units [6, 14, 15], although it should be stated that the 2D approximations of 3D cylindrical beds will lead to systematic deviations within the parameter space of interest [16] and that the simulation becomes very sensitive to exact cluster resolution when fast reactions are simulated [17]. The complete equation system can be viewed in [1].

### 4.1.1 Conservation equations

The continuity and momentum equations for the gas and solids phases are given below:

$$\frac{\partial}{\partial t}\left(\alpha_g \rho_g\right) + \nabla \cdot \left(\alpha_g \rho_g \vec{\upsilon}_g\right) = 0 \qquad \textbf{Equation 1}$$

$$\frac{\partial}{\partial t}\left(\alpha_g \rho_g \vec{\upsilon}_g\right) + \nabla \cdot \left(\alpha_g \rho_g \vec{\upsilon}_g \vec{\upsilon}_g\right) = -\alpha_g \nabla p + \nabla \cdot \bar{\bar{\tau}}_g + \alpha_g \rho_g \vec{g} + K_{sg}\left(\vec{\upsilon}_s - \vec{\upsilon}_g\right) \qquad \textbf{Equation 2}$$

$$\frac{\partial}{\partial t}\left(\alpha_s \rho_s\right) + \nabla \cdot \left(\alpha_s \rho_s \vec{\upsilon}_s\right) = 0 \qquad \textbf{Equation 3}$$

$$\frac{\partial}{\partial t}\left(\alpha_s \rho_s \vec{\upsilon}_s\right) + \nabla \cdot \left(\alpha_s \rho_s \vec{\upsilon}_s \vec{\upsilon}_s\right) = -\alpha_s \nabla p - \nabla p_s + \nabla \cdot \bar{\bar{\tau}}_s + \alpha_s \rho_s \vec{g} + K_{gs}\left(\vec{\upsilon}_g - \vec{\upsilon}_s\right) \qquad \textbf{Equation 4}$$

The solids stresses $\left(p_s \text{ and } \bar{\bar{\tau}}_s\right)$ are modelled according to the KTGF. Interphase momentum exchange $\left(K_{gs} = K_{sg}\right)$ was modelled according to the formulation of Syamlal and O'Brien [4]. The drag law is the most important factor which influences the particle size-related grid independence behaviour of the TFM and the full formulation is presented in Section 5.2.

Species are conserved only for the gas phase.

$$\frac{\partial}{\partial t}\left(\alpha_g \rho_g Y_{gi}\right) + \nabla \cdot \left(\alpha_g \rho_g \vec{\upsilon}_g Y_{gi}\right) = \nabla \cdot \alpha_g \vec{J}_{gi} + \alpha_g S_{gi} \qquad \textbf{Equation 5}$$

No energy conservation was included under the assumption of isothermal flow. This is usually a good assumption due to the excellent mixing achieved in fluidized bed reactors.

### 4.1.2 The kinetic theory of granular flows

The KTGF [2-4] was implemented to model solids stresses resulting from particle collisions and uncorrelated translations. Kinetic energy contained in the random particle motions is quantified in terms of granular temperature and can be written in conservation form as follows:

$$\frac{3}{2}\left[\frac{\partial}{\partial t}\left(\alpha_s \rho_s \Theta_s\right)+\nabla\cdot\left(\alpha_s \rho_s \vec{\upsilon}_s \Theta_s\right)\right]=\left(-p_s\bar{\bar{I}}+\bar{\bar{\tau}}_s\right):\nabla\vec{\upsilon}_s+\nabla\cdot\left(k_{\Theta_s}\nabla\Theta_s\right)-\gamma_{\Theta_s}+\phi_{gs} \qquad \textbf{Equation 6}$$

In the present study, this equation was solved in its algebraic form by neglecting the contributions of convection (second term on the left) and diffusion (second term on the right). This is a good assumption in dense and slow moving bubbling beds [18] since the local generation (first term on the right), dissipation due to inelastic collisions (third term on the right) [3] and damping by the primary phase (final term) [2] strongly outweigh contributions from convective and diffusive fluxes.

The granular temperature is subsequently used to calculate values of the solids viscosity which are used in the solids stress tensor. Bulk viscosity [3] and the three components of shear viscosity, collisional [2, 4], kinetic [2] and frictional [19], were considered in the calculations.

Normal stresses modelled according to the solids pressure used in Equation 4 as well as in Equation 6 is calculated according to Lun *et al.* [3]. The radial distribution function which is a measure of the average distance between particles is a central concept in the KTGF and is calculated according to Ogawa and Oshima [20].

### 4.1.3 Reaction kinetics

Reaction kinetics were implemented using the shrinking core model [21] with chemical kinetics as the rate limiting step (no internal or external mass transfer limitations). A simple, catalytic

conversion of gas species A to gas species B was simulated to occur on the surface of microscopic solid grains (*S*) within the particles used in the fluidized bed:

$$A + S \rightarrow B + S$$

The physical and chemical properties of species A and B were specified to be identical so that the reaction would not influence the hydrodynamics resulting in a non-linear interaction. This significantly simplifies the interpretation of results, enabling clearly decoupled conclusions regarding hydrodynamic and reactive grid independence to be drawn from each simulation.

When reaction rate control is assumed with the shrinking core model, the rate of consumption of species A on the surface of the unreacted core can be expressed as follows:

$$-\frac{dN_A}{dt} = \pi d_c^2 k C_A^n \qquad \textbf{Equation 7}$$

This relation can be rewritten in terms of a volumetric heterogeneous reaction rate that can be implemented into the CFD code:

$$R_H = -\frac{1}{V}\frac{dN_A}{dt} = \frac{6}{d_g}\alpha_s k C_A = \frac{6}{d_g}\alpha_s k\left(\frac{Y_A \rho_g}{M_A}\right) \qquad \textbf{Equation 8}$$

Equation 8 is formulated on the assumption that each particle is composed of much smaller grains ( $d_g = 1$ μm in this case) and that the reaction takes place at an equal rate on all the grains inside the particle and with no internal mass transport limitations. A first order reaction was simulated.

The hypothetical reaction rate constant in Equation 9 was implemented. Both the pre-exponential factor (0.1 m/s) and the activation energy (100 kJ/mol) are representative of real materials used in reacting fluidized bed systems such as the metal oxides used in chemical looping combustion.

$$k = 0.1\exp\left(-100000/RT\right) \quad \textbf{Equation 9}$$

The reaction rate in each cell (molar rate of change from species A to species B per unit volume) was then implemented as a source term into Equation 5. Since the species had identical properties and the reaction occurred in a 1:1 stoichiometric ratio, no mass or momentum source terms were required. The source term in Equation 5 was taken as $S_{gi} = R_H M_i$ for the product species (B) and $S_{gi} = -R_H M_i$ for the reactant species (A).

### 4.1.4 Boundary Conditions

A simple no-slip wall boundary condition was set for the gas phase. The Johnson and Jackson [22] boundary condition was used for the granular phase with a specularity coefficient $(\varsigma)$ of 0.5.

$$\vec{\tau}_s = -\frac{\pi}{6}\sqrt{3}\varsigma\frac{\alpha_s}{\alpha_{s,\max}}\rho_s g_{0,ss}\sqrt{\Theta_s}\vec{U}_{s,\|} \quad \textbf{Equation 10}$$

A velocity inlet condition was specified according the specific simulation run in question and was considered to be a function of the particle size. This was done according to the classic flow regime diagrams of Bi & Grace [23] by always taking the fluidization velocity that would lie in the middle of the bubbling fluidization regime, bisecting the boundaries posed by the minimum fluidization velocity and the critical velocity where turbulent fluidization commences. These boundaries are calculated as follows [23]:

$$\mathrm{Re}_{mf} = \sqrt{27.2^2 + 0.0408\mathrm{Ar}} - 27.2 \quad \textbf{Equation 11}$$

$$\mathrm{Re}_c = 1.24\mathrm{Ar}^{0.45} \quad \textbf{Equation 12}$$

using the Reynolds number $\left(\mathrm{Re} = \left(\rho_g U d_s\right)/\mu_g\right)$ and the Archimedes number $\left(\mathrm{Ar} = \left(\rho_g\left(\rho_s + \rho_g\right)g d_s^3\right)/\mu_g^2\right)$

.

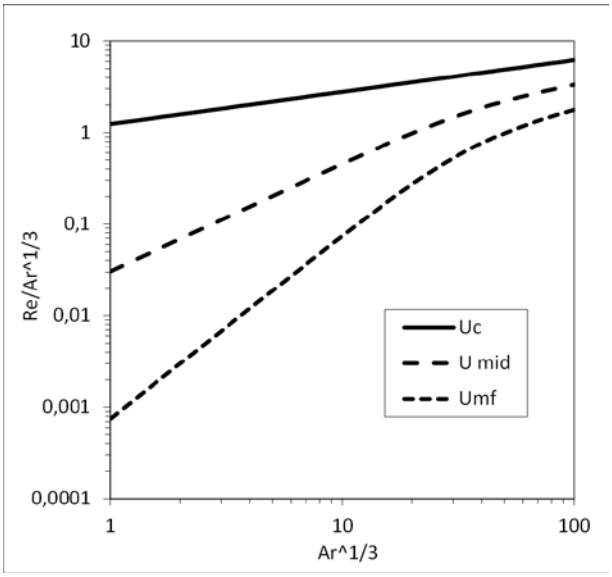


**Figure 1: The centreline of the bubbling fluidization regime used to specify the fluidization velocity as a function of particle size.**

As can be seen from Figure 1, the fluidization velocity (nondimensionalized as the Reynolds number) is linked to the particle size (nondimensionalized as the Archimedes number) according to the mid-line (designated as U mid in Figure 1). The line U mid is determined by calculating the nondimensionalized $\left(U^* = \mathrm{Re}/\mathrm{Ar}^{1/3}\right)$ minimum fluidization and critical velocities and then taking the geometric mean of these two extremes.

$$U^*_{mid} = \sqrt{U^*_{mf} \cdot U^*_c} \qquad \textbf{Equation 13}$$

Scaling the fluidization velocity as specified in Equation 13 was tested to result in very similar fluidization for bubbling fluidized beds using different particle sizes. The resulting fluidization velocities used for the five particle sizes considered in this study are given in Table 1.

**Table 1: Fluidization velocity (Equation 13) used for each particle size. The other physical properties used in Equation 13 are given in Table 2.**

| Particle size (μm) | Fluidization velocity (m/s) |
|---|---|
| 200 | 0.263 |
| 400 | 0.600 |
| 600 | 0.945 |
| 800 | 1.340 |
| 1000 | 1.730 |

The incoming gas consisted of pure reactant (species A). The outlet was specified as a pressure outlet at atmospheric pressure.

## 4.2 Flow solver and solver settings

The commercial software package, ANSYS FLUENT 13.0 [24] was used as the solver. The phase coupled SIMPLE scheme (extension of [25]) was used for pressure-velocity coupling and the higher order QUICK scheme [26] for the spatial discretization of all remaining equations. First order implicit temporal discretization was used to ensure stable and accurate solutions. It has been shown that 2$^{nd}$ order time discretization is necessary for accurate solution of fast-moving riser flows with the TFM [1], but this is not the case for dense bubbling beds where the vast majority of the bed moves very slowly. The timestep size was varied between different simulations according to the following formula: $\Delta t = \Delta / (20U)$ where $\Delta$ is the cell size and $U$ is the fluidization velocity.

## 4.3 Geometry and meshing

All simulations were carried out in simple rectangular 2D geometries meshed with structured grid cells. The 2D configuration was chosen in order to allow for the large number of simulations completed in this study. In addition, it has been recently found that 3D simulations show better grid-independence behaviour than 2D simulations [27], implying that conclusions from 2D simulations should be safely extendable to 3D simulations.

As illustrated in Figure 2, each geometry was divided into three zones: the bed zone comprising the bottom 40% of the reactor, a porous zone for the top 10% and a freeboard zone for the remaining 50% in between. The bed zone was used for patching in the initial solids bed and collecting time-averaged statistics within the bed region, while the porous zone was specified to ensure plug flow out of the reactor. This porous zone prevented backflows (which would have to be accurately specified) at the reactor outlet.

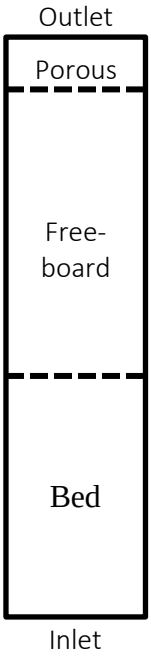


**Figure 2: Schematic of the simple 2D simulation domain.**

Many different geometry and mesh sizes were evaluated in the present study. The geometry size was scaled with the particle size in order to attain a trend of grid dependent behaviour with a reasonable number of grid cells. This was done because the grid independence behaviour of fluidized bed simulations is known to be very sensitive to changes in particle size and a wide range of particle sizes was investigated (200 – 1000 μm). If all simulations were carried out using an identical geometry size, the number of grid cells required to get reasonable bubble resolution with the finest particle size would be too expensive, while the coarsest particle size would probably achieve adequate bubble resolution at a grid size so coarse that it cannot even resolve the macroscopic flow structure within the reactor.

Therefore, the decision was made to scale the geometry size as a function of the particle size, while a constant aspect ratio of 5 was maintained. This was done according to the fluidization velocities reported in Table 1. Significant experimentation showed that a scaling of 1.5 times the fluidization velocity for the column width and 7.5 times the fluidization velocity for the column height resulted in reasonable grid sizes. Using this scaling, the geometry used for the coarsest particle size (1000 μm) was almost 7 times wider and taller than that used for the

smallest particle size (200 μm). Qualitative comparisons showed that this methodology resulted in good dynamic similarity between cases. This can also be quantitatively confirmed from the hydrodynamic results presented in Section 5.1 where the bed expansion ratio is around 1.6 for all cases (calculated from Table 4) and the standard deviation of the solids volume fraction around 0.2 (Table 5).

Meshing was carried out using perfectly square cells. For each particle size, at least 5 different grid sizes were evaluated, increasing the total cell count by a factor of two for each refinement. For the 2D geometry considered in this study, this implies a reduction in the cell size of $\sqrt{2}$ for each refinement. The five grid sizes considered for most cases resulted in cell counts along the width of the domain of 14, 20, 28, 40 and 57 cells. Two cases required simulations to be carried out at even finer grids in order to gather additional data. These cell counts were maintained for all grids used, thereby implying that the cell sizes used for the coarser particles were much larger than those used for the fine particles.

For the finer grids, hanging node adaptive grid refinement was used only in the lower parts of the geometry where the particles reside, in order to avoid large numbers of unnecessarily fine cells in the freeboard region where good resolution is not necessary.

## 4.4 Initial conditions

Simulations were initialized with no solid particles, no reactant gas (only product gas) and zero velocity. The bed material was subsequently patched into the lower 40% of the geometry, implying that the initial patched region containing bed material had an aspect ratio of 2. The initial solids volume fraction patched in was 0.4.

Simulations were then run for a period sufficiently long to allow the gas to pass twice through the entire length of the domain at the superficial injection velocity. This time period was found to be sufficiently long to ensure quasi-steady flow behaviour (according to the measures

outlined in Section 4.6.1) and the solution at this point was used as the initial condition for commencing time-averaging.

## 4.5 Simulation summary

A summary of the physical properties and simulation parameters are given in Table 2.

**Table 2: Physical properties and simulation parameters**

| | |
|---|---|
| Gas density (A and B) | 0.3 kg/m$^3$ |
| Gas viscosity (A and B) | 4.5x10$^{-5}$ kg/m·s |
| Particle density | 2500 kg/m$^3$ |
| Grain diameter | 1 μm |
| Bed aspect ratio | 5 |
| Particle-particle restitution | 0.9 |
| Specularity coefficient | 0.5 |
| Initial solids packing | 0.40 |
| Maximum packaging limit | 0.63 |

## 4.6 Data collection and processing

This study was conducted with the aim of getting a holistic picture of the sensitivity of grid independence behaviour to changes in particle size. Three performance measures were therefore collected and processed in a very specific manner.

### 4.6.1 Performance measures

The three performance measures collected in this work are listed below. All performance measures were calculated from time averaged data collected over a time period sufficiently long for the fluidizing gas to pass through the reactor 20 times.

#### *4.6.1.1 Reactor performance*

This is the primary performance measure of interest in fluidized bed reactors and is calculated as follows from the average mass fraction $\left(Y_{A,outlet}\right)$ of reactant (A) exiting the reactor unreacted (averaged in time and space over the reactor outlet):

$$X = -\log\left(Y_{A,outlet}\right)$$ **Equation 14**

This measure can be interpreted as a measure of the residence time required to convert the reactant to a certain degree when all other factors influencing reaction rate are kept constant. In this case, for a first order reaction, the rate of change of the reacting species mass fraction would be expressed as follows: $dY/dt = -CY$ which can be integrated from $Y_0 = 1$ at $t_0 = 0$ to find the time $(t)$ at a certain final conversion $(Y)$ as $t = -C^{-1}\ln(Y)$. In this case it was assumed that the constant $C^{-1} = \log(e)$ in order to express time required to reach a given conversion $(Y)$ as $t = -\log(Y)$. This measure was used as the primary indicator of reactor performance (Equation 14).

The base 10 logarithm was chosen simply to make the results easier to interpret. For instance, 0% conversion would return a reactor performance of $-\log(1) = 0$, 90% conversion would return a reactor performance of $-\log(0.1) = 1$, 99% conversion a reactor performance of $-\log(0.01) = 2$ etc. In practice, this measure linearizes reactor performance achieved from a first order reaction and makes it possible to distinguish between cases which achieve high conversions.

#### *4.6.1.2 Expanded bed height*

This hydrodynamic performance measure was calculated as the height at which the solids volume fraction (averaged in time and cross-stream space) is 0.05. Below this line, the dense bed region exists at much higher solids volume fractions and above this line, the freeboard region exists at volume fractions close to zero. This measure was therefore found to be a good indicator of the expanded bed height. From a reactor performance point of view, this performance measure indicates the residence time of the gas inside the bed. A more compact bed has a doubly reductive influence on gas residence time by shortening the distance that the

gas can travel inside the bed and by increasing the actual gas velocity due to a decrease in gas voidage. From a hydrodynamic point of view, it indicates the degree of momentum coupling between the gas and the solids. A greater bed expansion implies that the overall drag force experienced by the particles is larger.

#### *4.6.1.3 Phase segregation*

This performance measure was quantified as the volume average of the RMS (root mean square) of the solids volume fraction over the bed region (lower 40% of the physical height of the reactor). A high value of the RMS indicates large volume fraction fluctuations during the averaging process and therefore significant volume fraction segregation. From a reactor performance point of view, this performance measure indicates the quality of gas-solid contact achieved within the reactor. A high degree of phase segregation implies poor contact between the solids and the gas and thereby poorer reactor performance.

### 4.6.2 Data processing

The data collected for the above mentioned performance measures was subsequently analysed in order to quantify the grid independence behaviour for each particle size. This was done by assuming the performance measure to exhibit idealized grid dependence behaviour where the simulation accuracy decreases exponentially as the grid is coarsened.

The grid size was linearized by the following formula for this purpose:

$$\Delta_{lin} = \log_2\left(\frac{56.57}{N_x}\right) \qquad \textbf{Equation 15}$$

Here, $N_x$ is the number of width-wise grid cells which was taken as 14, 20, 28, 40 and 57 for most cases. For these five grid spacings, Equation 15 returns values of 2, 1.5, 1, 0.5 and 0 when rounded to the nearest tenth, thereby providing a linear grid spacing parameter.

The value of each performance measure $(X)$ collected on a specific grid using a specific particle size was normalized by the value of that performance measure on another grid spacing $(X_{base})$ as shown in Equation 16. The selection criterion for this base case will be discussed shortly. The normalized reactor performance, for example, would be expressed as a percentage as follows:

$$X_{norm} = \frac{X}{X_{base}} \times 100\% \qquad \textbf{Equation 16}$$

A typical plot of the normalized performance measure against the linearized grid spacing is given in Figure 3 where the expected exponential decay in solution accuracy with increasing grid spacing is observed.

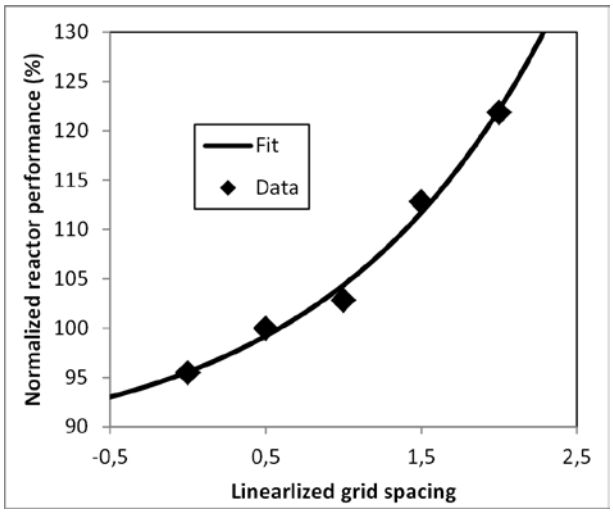


**Figure 3: Grid dependence behaviour of the reactor performance for the 600 µm case.**

An exponential growth function in the form $X_{norm} = A + \exp(B + C \cdot \Delta_{lin})$ was fit to all the reactor performance cases utilized in this study with an $R^2$ value greater than 0.97. This fitted function was then used to calculate the grid spacing at which a doubling of the cell size would change the normalized solution ( $X_{norm}$ in Equation 16) by only 10%. The exponential growth function was differentiated for this purpose:

$$\frac{dX_{norm}}{d\Delta_{lin}} = C \exp(B + C \cdot \Delta_{lin}) \qquad \textbf{Equation 17}$$

The linearized grid spacing when the rate of change in the normalized reactor performance is 10% per doubling of the grid spacing is then calculated as follows:

$$\Delta_{lin} = \frac{\ln\left(\frac{dX_{norm}}{d\Delta_{lin}}\right) - \ln(C) - B}{C} \qquad \textbf{Equation 18}$$

where $dX_{norm}/d\Delta_{lin}$ is taken as 10% (representing 10% change per doubling of the grid spacing) and the constants $B$ and $C$ are calculated to provide the best fit to the simulation data (e.g. the fit in Figure 3). Note that $d\Delta_{lin} = 1$ represents a doubling of the grid spacing.

This process was used iteratively to set the base case to which the performance measures were normalized ( $X_{base}$ Equation 16) as the data point closest to the "10% change per doubling of the grid spacing" point calculated in Equation 18. In this way, it is ensured that the 10% would be based on a realistic normalization. In Figure 3, for example, the most suitable base case was found to be the one having 40 cells along the width of the reactor, i.e. a linearized grid spacing of 0.5 (Equation 15).

Finally, this information is used in Equation 18 to calculate the final linearized grid spacing at which the solution would change by only 10% per doubling of the grid spacing. This cell size was then taken as the "grid independent" cell size for the specific particle size under investigation. It is conceded that a stricter criterion would normally be used to judge grid independence, but this study required significant variations between grids in order to increase the ratio of systematic variance over error variance and guarantee a good fit such as given in Figure 3. Therefore, grid spacings that still showed significant grid dependence effects were intentionally chosen.

# 5 Results and discussion

Results will be presented in three sections: a look at the grid independence behaviour of the TFM, an analysis of the influence of the particle relaxation time on the grid independence behaviour and a discussion about the implications for large scale simulations.

## 5.1 Grid independence behaviour of the TFM

Results from the three performance measures on different grids for different particle sizes are given below:

**Table 3: Reactor performance results for different grid resolutions (expressed as the number of width-wise cells) using different particle sizes. Both the actual (top row) and normalized (bottom row) results are reported for each particle size.**

| Particle size (μm) | 14 cells | 20 cells | 28 cells | 40 cells | 57 cells | 80 cells | 113 cells | 160 cells | 226 cells |
|---|---|---|---|---|---|---|---|---|---|
| 200 | | | | | 2.08 | 1.82 | 1.60 | 1.46 | 1.39 |
| | | | | | 149.9 | 131.0 | 115.5 | 105.3 | 100.0 |
| 400 | | 2.80 | 2.47 | 2.30 | 2.06 | 1.98 | | | |
| | | 141.4 | 124.7 | 116.1 | 104.1 | 100.0 | | | |
| 600 | 3.43 | 3.03 | 2.88 | 2.75 | 2.53 | | | | |
| | 124.9 | 110.2 | 104.7 | 100.0 | 92.1 | | | | |
| 800 | 3.57 | 3.30 | 3.01 | 2.93 | 2.80 | | | | |
| | 121.9 | 112.8 | 102.8 | 100.0 | 95.5 | | | | |
| 1000 | 3.70 | 3.29 | 3.20 | 3.09 | 2.94 | | | | |
| | 115.5 | 102.7 | 100.0 | 96.5 | 91.9 | | | | |

When the procedure described in Section 3.6.2 is applied to the data in Table 3, the grid size achieving the prescribed grid independence criterion (10% change with doubling of the cell size) can be calculated for each particle size. The results are displayed in Figure 4.

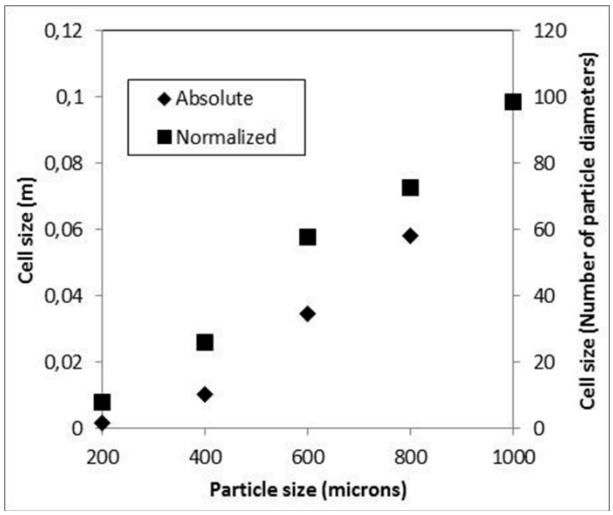


**Figure 4: Cell sizes achieving sufficiently grid independent reactor performance results as a function of particle size. The grid size is expressed both in terms of absolute size (left y-axis) and normalized size (right y-axis).**

The first observation from Figure 4 is that the traditional grid independence guideline of taking the cell size as a specific factor of particle size is not satisfied. When the cell size is normalized in terms of the number of particle diameters, grid independence is achieved on a cell size of 7.8 particle diameters for the 200 µm particles and a cell size of 98.4 particle diameters for the 1000 µm particles – a difference of more than one order of magnitude.

When looking at the absolute cell size, the requirement for 200 µm particles (1.46 mm cells) and 1000 µm particles (93.38 mm cells) differ by a factor of 63.3. When conducting a well resolved 2D simulation on a constant domain size, the simulation time required to solve a fixed amount of physical time is inversely proportional to the cube of the cell size because the timestep must reduce proportionally to the cell size. If the same reactor is simulated with 200 µm and 1000 µm particles, therefore, the simulation will be $63.3^3 = 253{,}636$ times faster for the 1000 µm particles than for the 200 µm particles. If the same relationship holds in 3D, this ratio will be $63.3^4 = 16{,}055{,}167$.

It has been known for a long time that direct simulations of fine powders are more expensive, but the sheer magnitude of this effect has not been sufficiently emphasized. The implication is that, even while well resolved simulations of fine powders will remain out of range for a long

time to come, industrial scale systems using much larger particles can readily be simulated using today's computer resources. After all, the data seems to suggest that a factor of five increase in particle size will allow for a factor of 16 million reduction in the required simulation time in 3D. This will be discussed in more detail at a later stage (Figure 15 and Figure 16).

The reason for this very large effect of particle size on grid independence behaviour of the reactor performance is two-fold. Firstly, it is expected that the cluster size to be resolved should be a function of the particle relaxation time. Smaller particles can follow much smaller eddies because they relax to the flow very quickly. These particles therefore perform very fine scale motions and can circumvent a particle cluster along the streamlines flowing around it. Larger particles, however, are poorly coupled to the carrier phase and cannot circumvent clusters in this way. They therefore collide with most clusters they encounter joining in the bulk of the cluster.

The naturally occurring cluster size will be the primary factor influencing the grid independent cell size. Particles with a very small relaxation time will require very strong streamline curvature in order to depart sufficiently from the streamline in order to join in the bulk of a cluster. If the grid is not sufficiently fine to resolve such rapid streamline curvature, the particle will never depart from the carrier phase and clusters will not form. This is very clearly seen when running coarse grid simulations with fine powders (see Figure 7 for example). Particles with a long relaxation time, on the other hand, only require a slight degree of streamline curvature to depart significantly from the carrier phase, collide with other particles and form clusters.

Secondly, the resolution of particle structures becomes less important from a mass-transfer point of view as the particle size increases. Particle structures consisting of very fine particles are virtually impervious to the fluidizing gas, implying that, for a reactive situation, the reacting

gas cannot easily penetrate into the cluster and virtually all of the reaction has to occur on the surface of the cluster. Accurate resolution of particle structures is therefore very important for model accuracy in this case and will lead to large over-predictions of gas-solid contact (and therefore overall reactor performance) if the gas-solid interface is smeared out through poor numerical resolution. For larger particles, on the other hand, a cluster of particles is much more permeable to the fluidizing gas, allowing large quantities of reactant to penetrate into the cluster and react with the particles within. Since only a fraction of the reaction now occurs on the surface of the cluster, the correct resolution of this surface becomes less important for model accuracy.

These two effects are expected to combine to cause the very large observed effect of particle size on grid independence behaviour and will be further analysed in the subsequent section where grid independence will be quantitatively linked to the drag law via the particle relaxation time.

The two separate effects just discussed can be split up for better analysis by also looking at hydrodynamic performance measures. Data collected for the expanded bed height performance measure is reported in Table 4.

**Table 4: Expanded bed height results for different grid resolutions (expressed as the number of width-wise cells) using different particle sizes. Both the actual (top row) and normalized (bottom row) results are reported for each particle size.**

| Particle size (μm) | 14 cells | 20 cells | 28 cells | 40 cells | 57 cells | 80 cells | 113 cells | 160 cells | 226 cells |
|---|---|---|---|---|---|---|---|---|---|
| 200 | | | | | 0.946 | 0.905 | 0.874 | 0.851 | 0.84 |
| | | | | | 112.6 | 107.7 | 104.0 | 101.3 | 100.0 |
| 400 | | 2.009 | 1.975 | 1.95 | 1.922 | 1.916 | | | |
| | | 104.9 | 103.1 | 101.8 | 100.3 | 100.0 | | | |
| 600 | 2.982 | 2.952 | 2.969 | 2.963 | 2.964 | | | | |
| | 100.6 | 99.6 | 100.2 | 100.0 | 100.0 | | | | |
| 800 | 4.116 | 4.178 | 4.202 | 4.213 | 4.241 | | | | |
| | 97.1 | 98.5 | 99.1 | 99.3 | 100.0 | | | | |
| 1000 | 5.280 | 5.386 | 5.431 | 5.470 | 5.516 | | | | |
| | 95.7 | 97.6 | 98.5 | 99.2 | 100.0 | | | | |

The first observation from Table 4 is that grid independence behaviour for the expanded bed height performance measure is much better than it is for the reactor performance (Table 3). The 200 μm case is the only one showing sufficiently large grid dependence behaviour. For this reason, a grid independence trend such as the one shown in Figure 4 could not be established for the bed height.

It is also interesting to observe that the grid dependency response of the expanded bed height is different for fine and coarse particles. For the 200 μm particles, the bed over-expands at poor resolutions because the fine scale clusters which slip much more readily relative to the fluidizing gas are not sufficiently resolved. This is a well-known effect [1, 6]. For the 1000 μm particles, on the other hand, the effect seems to be opposite in that the bed under-expands slightly at lower resolutions. An analysis of this effect is postponed to the next section.

Grid independence behaviour with regard to the second hydrodynamic performance measure, phase segregation, is given in Table 5.

**Table 5: Phase segregation results for different grid resolutions (expressed as the number of width-wise cells) using different particle sizes. Both the actual (top row) and normalized (bottom row) results are reported for each particle size.**

| Particle size (μm) | 14 cells | 20 cells | 28 cells | 40 cells | 57 cells | 80 cells | 113 cells | 160 cells | 226 cells |
|---|---|---|---|---|---|---|---|---|---|
| 200 | | | | | 0.189 | 0.207 | 0.220 | 0.228 | 0.235 |
| | | | | | 85.9 | 93.7 | 100.0 | 103.5 | 106.4 |
| 400 | | 0.160 | 0.185 | 0.200 | 0.210 | 0.218 | | | |
| | | 80.2 | 92.6 | 100.0 | 105.2 | 109.0 | | | |
| 600 | 0.152 | 0.172 | 0.190 | 0.202 | 0.209 | | | | |
| | 75.4 | 85.3 | 94.3 | 100.0 | 103.8 | | | | |
| 800 | 0.150 | 0.178 | 0.194 | 0.203 | 0.210 | | | | |
| | 77.3 | 91.8 | 100.0 | 104.3 | 107.8 | | | | |
| 1000 | 0.155 | 0.179 | 0.195 | 0.202 | 0.208 | | | | |
| | 79.6 | 92.1 | 100.0 | 103.7 | 106.8 | | | | |

It is immediately evident that this data set contains much more variance than that for the bed expansion and a meaningful trend can therefore be established in Figure 5. When comparing Figure 5 to Figure 4, it can be seen that the grid independence behaviour of the simulation with

respect to reactor performance and phase segregation is very similar. This confirms the central importance of correct predictions of the gas-solid contact in fluidized bed reactor simulations.

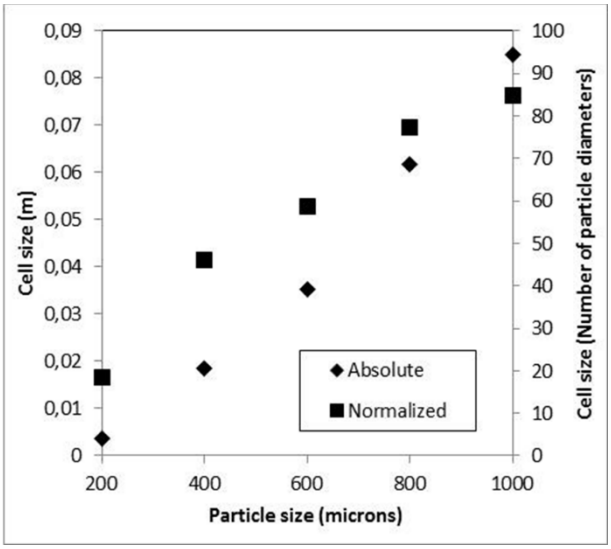


**Figure 5: Cell sizes achieving sufficiently grid independent phase segregation results as a function of particle size. The grid size is expressed both in terms of absolute size (left y-axis) and normalized size (right y-axis).**

The question of the importance of cluster permeability in reactor performance grid independence behaviour can now be further examined. When grid independent cell sizes for phase segregation are compared to grid independent cell sizes for reactor performance, the sensitivity of reactor performance to correct modelling of phase segregation can be assessed. In effect, such a comparison will show the extent to which accurate cluster resolution (the first effect discussed previously) controls the predicted reactor performance and thereby indicate the importance of the cluster permeability (the second effect discussed previously).

If these two performance measures show identical grid independence behaviour, it can be assumed that the prediction of reactor performance is only influenced by the degree to which particle clusters are resolved. If they respond differently, however, the cluster permeability also plays a significant role. In order to further investigate this notion, the ratio between the grid independent cell sizes for phase segregation and reactor performance is plotted in Figure 6 for different particle sizes.

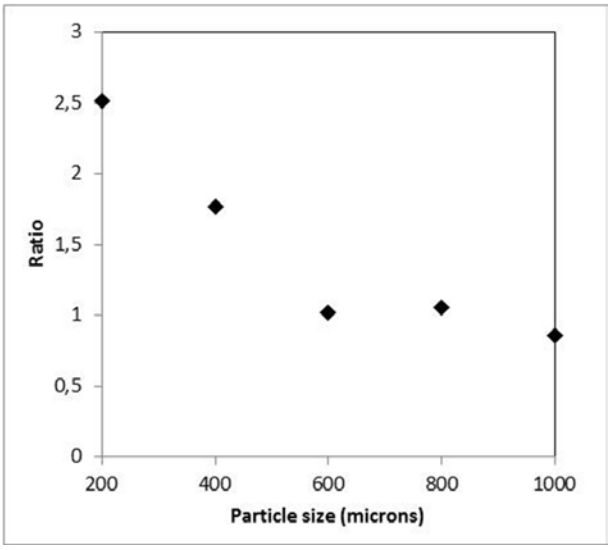


**Figure 6: The ratio of the sufficiently grid independent cell size for phase segregation to the sufficiently grid independent cell size for reactor performance calculated from the results in Figure 4 and Figure 5.**

It is clear that this ratio increases towards smaller particle sizes. This implies that, for small particle sizes, the cell size required for adequate reactor performance (degree of conversion) predictions is smaller than the cell size required to achieve adequate phase segregation (2.5 times smaller for 200 μm according to Figure 6). This is due to the low permeability of particle clusters consisting of smaller particles, forcing the reaction to occur on the surface of the cluster. In such cases, the gas-solid interface has to be resolved to a very high degree of accuracy in order to correctly predict reactor performance.

For larger particle sizes, this ratio is around 1, implying that the effect of cluster permeability becomes negligible. The reason for this is simply that clusters of 1 mm particles will be much more permeable to the fluidizing gas, allowing reacting species to easily penetrate deep into the cluster so that the reaction occurs throughout the cluster. The accurate resolution of the gas-solid interface therefore becomes much less important. This is just another indication that the accurate numerical solution of fluidized bed reactors using larger particle sizes is much easier and cheaper to complete than those using finer powders.

## 5.2 Influence of the particle relaxation time on grid independence behaviour

This section quantifies grid independence behaviour of the TFM using the particle relaxation time calculated according to the drag law implemented in this study. The full formulation of the drag law used in this study [4] is provided below.

$$C_D = \left( 0.63 + \frac{4.8}{\sqrt{\mathrm{Re}_s / \upsilon_{r,s}}} \right)^2 \qquad \textbf{Equation 19}$$

$$\upsilon_{r,s} = 0.5\left( A - 0.06\,\mathrm{Re}_s + \sqrt{\left(0.06\,\mathrm{Re}_s\right)^2 + 0.12\,\mathrm{Re}_s\left(2B - A\right) + A^2} \right) \qquad \textbf{Equation 20}$$

$$A = \alpha_g^{4.14} \qquad \textbf{Equation 21}$$

$$\begin{aligned} B &= 0.8\alpha_g^{1.28} \qquad \alpha_g \le 0.85 \\ B &= \alpha_g^{2.65} \qquad \alpha_g > 0.85 \end{aligned} \qquad \textbf{Equation 22}$$

$$\mathrm{Re}_s = \frac{\rho_g d_s \left| \vec{\upsilon}_s - \vec{\upsilon}_g \right|}{\mu_g} \qquad \textbf{Equation 23}$$

$$f = \frac{C_D\,\mathrm{Re}_s\,\alpha_g}{24\upsilon_{r,s}^2} \qquad \textbf{Equation 24}$$

$$K_{gs} = K_{sg} = \frac{\alpha_s \rho_s f}{\tau_{s_S}} \qquad \textbf{Equation 25}$$

$$\tau_{s_S} = \frac{\rho_s d_s^2}{18\mu_g} \qquad \textbf{Equation 26}$$

In the previous section, it was reasoned that cluster resolution in the model should be a function of the particle relaxation time because particles need to be able to deviate significantly from the gas streamlines in order to collide and form clusters. For quantifying this effect, one cannot simply use the Stokes relaxation time (Equation 26) because two additional highly significant effects play a part in this case: high Reynolds number effects and hindered settling. The chosen drag law captures these effects in the formulation of Equation 24 and this relation can now be used to calculate the real particle relaxation time as follows:

$$\tau_s = \frac{\tau_{s_S}}{f} \qquad \textbf{Equation 27}$$

The calculation of the *f* function requires a specification of the slip velocity in the calculation of the Reynolds number (Equation 23). In order to calculate this slip velocity, a simple steady state, fully periodic simulation was run where the gas phase velocity was fixed at zero and a pressure gradient equal to the weight of the solids was implemented. The steady state downwards solids velocity was then taken as the slip velocity. This simple simulation was run for various combinations of particle size and volume fraction with results reported in Table 6.

**Table 6: Slip velocities (m/s) for various combinations of particle size and solids volume fraction.**

| Solids volume fraction | 200 µm particles | 400 µm particles | 600 µm particles | 800 µm particles | 1000 µm particles |
|---|---|---|---|---|---|
| 1E-06 | 0.957 | 2.747 | 4.631 | 6.412 | 8.023 |
| 0.1 | 0.625 | 1.85 | 3.211 | 4.546 | 5.801 |
| 0.2 | 0.392 | 1.24 | 2.274 | 3.331 | 4.341 |
| 0.3 | 0.236 | 0.842 | 1.684 | 2.584 | 3.458 |
| 0.4 | 0.134 | 0.564 | 1.236 | 1.981 | 2.711 |
| 0.5 | 0.0718 | 0.372 | 0.893 | 1.487 | 2.072 |
| 0.6 | 0.0361 | 0.242 | 0.627 | 1.075 | 1.519 |
| 0.63 | 0.0291 | 0.211 | 0.559 | 0.964 | 1.367 |

The fidelity of this method was evaluated by testing the slip velocities for a solids volume fraction of 0.63 against minimum fluidization velocities calculated by the model. The match was almost perfect, implying that this method gives accurate representations of the steady state slip velocity.

It is possible, however, that instantaneous slip velocities in regions of strong acceleration or deceleration in the fluidized bed might be significantly different from the steady state values reported in Table 6. The slip velocities returned by the simplified simulation should therefore only be seen as an approximate ensemble average which facilitate the practically feasible calculation of the particle relaxation time as a function of particle size and solids volume fraction.

By using these slip velocities, the real particle relaxation times can be estimated for each of the cases in Table 6 using Equation 27. These data are reported in Table 7.

**Table 7: Particle relaxation times (s) for various combinations of particle size and solids volume fraction.**

| Solids volume fraction | 200 µm particles | 400 µm particles | 600 µm particles | 800 µm particles | 1000 µm particles |
|---|---|---|---|---|---|
| 1E-06 | 0.0890 | 0.259 | 0.442 | 0.620 | 0.793 |
| 0.1 | 0.0654 | 0.207 | 0.382 | 0.568 | 0.753 |
| 0.2 | 0.0468 | 0.163 | 0.325 | 0.509 | 0.698 |
| 0.3 | 0.0324 | 0.127 | 0.276 | 0.451 | 0.633 |
| 0.4 | 0.0217 | 0.100 | 0.237 | 0.403 | 0.578 |
| 0.5 | 0.0141 | 0.080 | 0.206 | 0.363 | 0.530 |
| 0.6 | 0.0090 | 0.065 | 0.181 | 0.328 | 0.485 |
| 0.63 | 0.0078 | 0.061 | 0.174 | 0.318 | 0.472 |

The first insight from Table 7 is that the hindered settling effect becomes much larger at smaller particle sizes. This is seen as the primary reason why fine particle sizes require such small particle sizes to be accurately simulated. For the 200 µm particles for example, a particle travelling in a very particle-lean region will have a relaxation time in the order of 0.09 s and will therefore be able to deviate significantly from the carrier phase, collide with other particles and begin forming clusters. As the volume fraction increases, however, the particle relaxation time decreases rapidly to only 0.008 s, more than one order of magnitude smaller than the relaxation time in particle-lean regions. Thus, as clusters begin forming, particles become less able to deviate from the streamlines and form denser clusters. In other words, in regions where the particle volume fraction becomes higher, more pronounced streamline curvature needs to be resolved before the particles can deviate from streamlines and cause further phase segregation.

This ever-increasing resistance to further phase segregation as clusters are gradually formed is seen as the primary reason for the grid dependence behaviour typically observed in fluidized bed simulations of finer particles. This is illustrated in Figure 7.

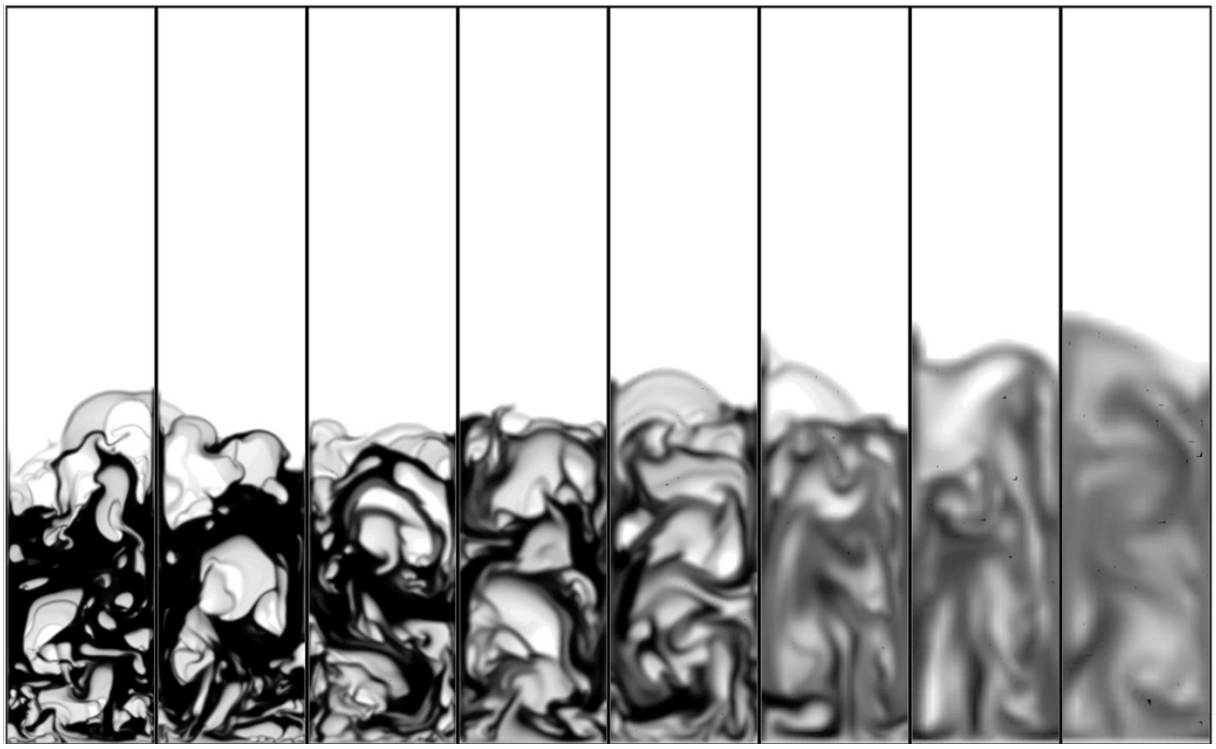

**Figure 7: Instantaneous phase solids phase volume fractions for the 200 µm particles in domains containing (from left to right) 226, 160, 113, 80, 57, 40, 28 and 20 width-wise cells.**

It is clear that sufficient streamline curvature is not resolved on the coarser meshes, implying that particles cannot deviate sufficiently from the streamlines in order to collide and cause further phase segregation. For this reason, the majority of particle structures fall below maximum packing on the mesh with 57 width-wise cells and continue to reduce in volume fraction as the grid is coarsened further. Further coarsening of the grid would eventually result in a virtually uniform particle distribution.

This strong hindered settling influence decreases with increases in particle size though. As shown in Figure 8, the decrease in particle relaxation time from a freely settling particle to a particle at maximum packing decreases significantly as the particle size is increased.

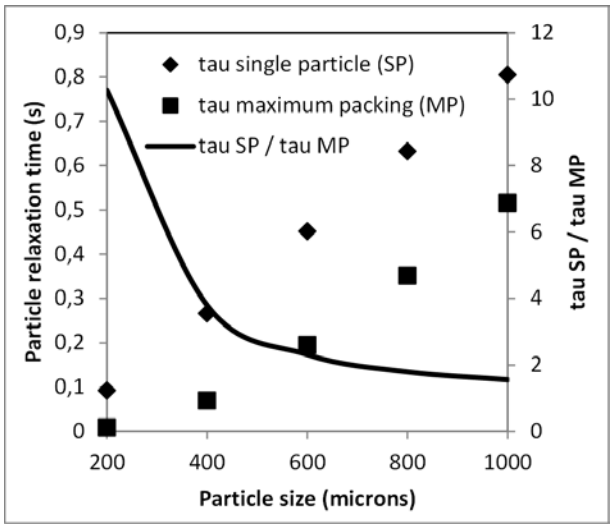


**Figure 8: The particle relaxation times (tau) for a single particle (SP) and a particle at maximum packing (MP) (left y-axis) as well as the ratio between these two quantities (right y-axis).**

In the light of the strong theoretical influence of particle relaxation time on cluster formation, it can be reasoned that the particle relaxation time should be a good predictor of the cell size required for phase segregation grid independence. This relation was confirmed by plotting the grid independent cell sizes in Figure 5 together with the particle relaxation times at the five different cell sizes investigated as shown in Figure 9.

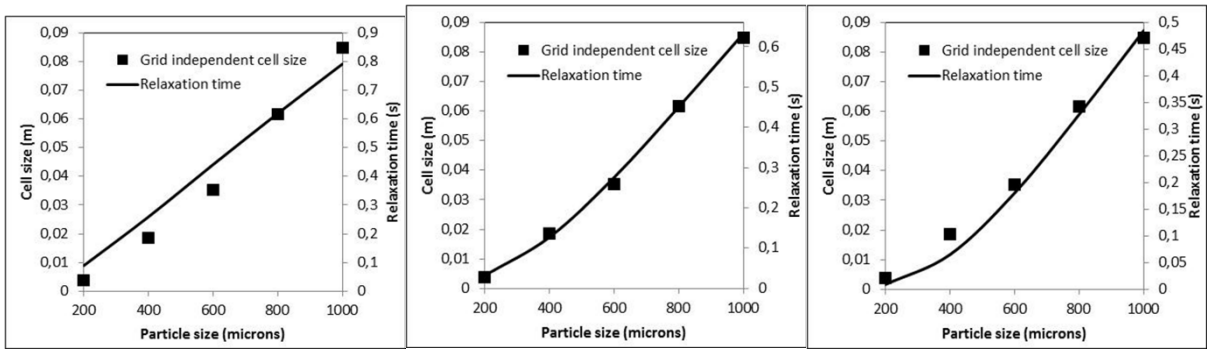


**Figure 9: The relation between the cell size for phase segregation grid independence and the particle relaxation time at particle volume fractions of 1e-6 (left), 0.3 (middle) and 0.6 (right).**

It is clear that the particle relaxation time at maximum packing is a very strong predictor of the cell size required for phase segregation grid independence and that the best fit is achieved with a particle relaxation time calculated at a volume fraction of 0.3. In order to quantify this relation, these two properties can be plotted against each other and proportionality can be established as shown in Figure 10.

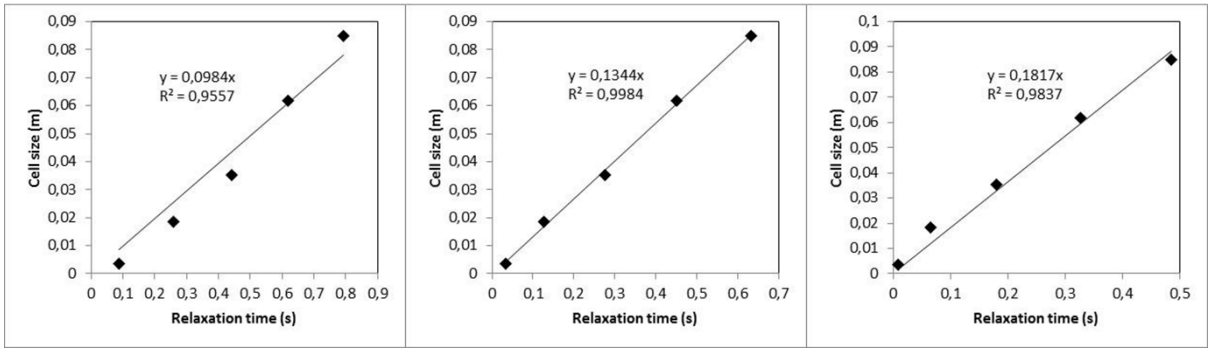


**Figure 10: Proportionality between the cell size required for phase segregation grid independence and the particle relaxation time at particle volume fractions of 1e-6 (left), 0.3 (middle) and 0.6 (right).**

It is clear that the grid independent cell size can be predicted as 0.13 times the particle relaxation time at a particle volume fraction of 0.3 with a high degree of accuracy ($R^2$ = 0.9984). The influence of the particle volume fraction at which the particle relaxation time is calculated on the quality of the fit can be better visualized in Figure 11.

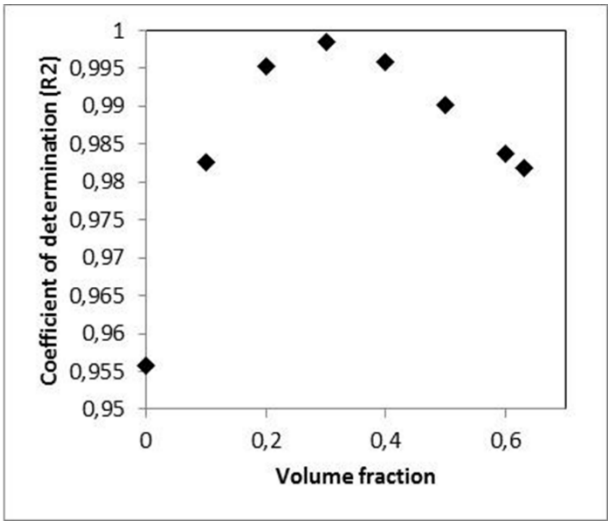


**Figure 11: The correlation quality ($R^2$) for the fit between the cell size for phase segregation grid independence and the particle relaxation time calculated for different phase volume fractions.**

The data shows that the best correlation between the grid independent cell size and the particle relaxation time occurs when the relaxation time is calculated at a volume fraction around 0.3. This result suggests that the sharpest streamline curvature that must be resolved in order to get the phases to segregate occurs around a volume fraction of 0.3. It should be emphasized that this is not a fundamental conclusion and further investigations are required to better understand the reasons behind the trend in Figure 11. The value of 0.3 should therefore not be taken as a generic grid independence guideline before more detailed investigations are completed.

Grid independence behaviour of the other two dependent variables investigated in this study (the expanded bed height and the reactor performance) is likely to be different since the resolved physics impacting these variables differs from the resolved physics impacting the phase segregation.

Unfortunately, no trend could be established for the bed expansion data given in Table 4 because of two competing effects on grid independence behaviour. No quantification is therefore possible in this case, but the two competing effects will be discussed in a little more detail. As seen in Figure 7, the degree of clustering goes down when the grid is coarsened, but so does the volume fraction inside clusters. Clustering reduces the effective interphase momentum transfer by binding small particles together in a larger entity which slips much more easily against a fluidizing gas stream. More clustering as resolved by a finer grid will therefore decrease bed expansion. On the other hand, less dense clusters (as solved on a coarse grid) will also reduce effective interphase momentum exchange by lowering the hindered settling effect, thereby increasing the effective slip velocity as shown in Table 6.

These are the two competing effects which make the bed expansion data hard to interpret. Upon refinement of the grid, clustering increases to decrease effective interphase momentum transfer, but at the same time, cluster density increases to increase effective interphase momentum transfer. From the data in Table 4, it can be seen that the clustering effect is strongest for small particles, while the cluster density effect becomes somewhat superior at larger particle sizes. This is the result of a transition from Geldart B particles (where bubbles move faster than gas in the suspension) to Geldart D particles (where gas in the suspension flows faster than the bubbles). For Geldart D particles (the 600, 800 and 1000 μm particles investigated in this study), gas flow through the suspension becomes more dominant and hence the cluster density effect starts to dominate.

When running reactive simulations, however, this possibility to correctly solve the expanded bed height even on very coarse meshes becomes largely irrelevant simply because phase segregation must be correctly resolved in order to capture the mass transfer limitation. The degree of bed expansion will influence the gas residence time inside the bed and therefore also the reactor performance, but a previous study [16] showed that the mass transfer effect was much more influential than this residence time effect. For this reason, the reactor performance grid independence behaviour was even more stringent than that for phase segregation.

Indeed, when looking at reactive grid independence, the two competing effects just discussed are actually compounding. Upon refinement of the grid, clustering increases to increase the phase segregation and thereby increase the effective mass transfer limitation in the reactor and, at the same time, cluster density becomes higher to further increase the mass transfer resistance by making it harder for the gaseous reactant to penetrate into the cluster. Both of these effects are controlled by the drag law and the particle relaxation time should therefore also be a good predictor of the cell size required for reactor performance grid independence.

In order to evaluate this theory, the same strategy used to compile Figure 11 was used to find the volume fraction at which the particle relaxation time should be calculated.

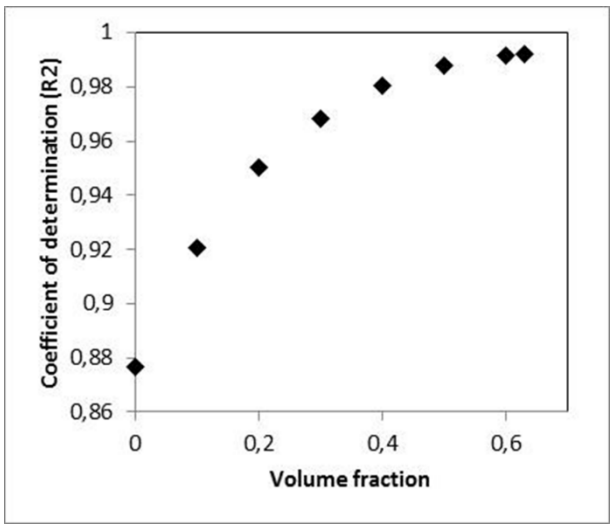


**Figure 12: The correlation quality ($R^2$) for the fit between the cell size for reactor performance grid independence and the particle relaxation time calculated for different phase volume fractions.**

Figure 12 shows that the best is now found at maximum packing. This fit is better visualized in Figure 13.

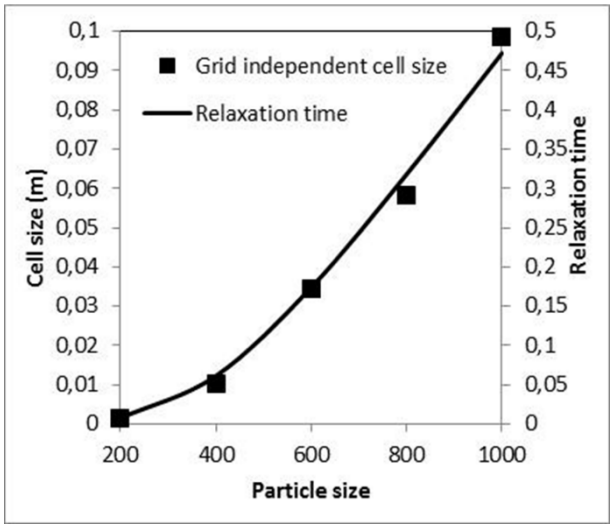


**Figure 13: The relation between the cell size for reactor performance grid independence and the particle relaxation time at maximum packing.**

The reason for the dependence on the particle relaxation time at maximum packing can be found from Figure 14. It is clearly shown that a large fraction of the reaction takes place on the gas/solids interface. If the gas/solids interface is not resolved sufficiently accurately and is smeared out significantly, the reaction rate will be over-predicted because of an artificially high amount of gas/solid contact.

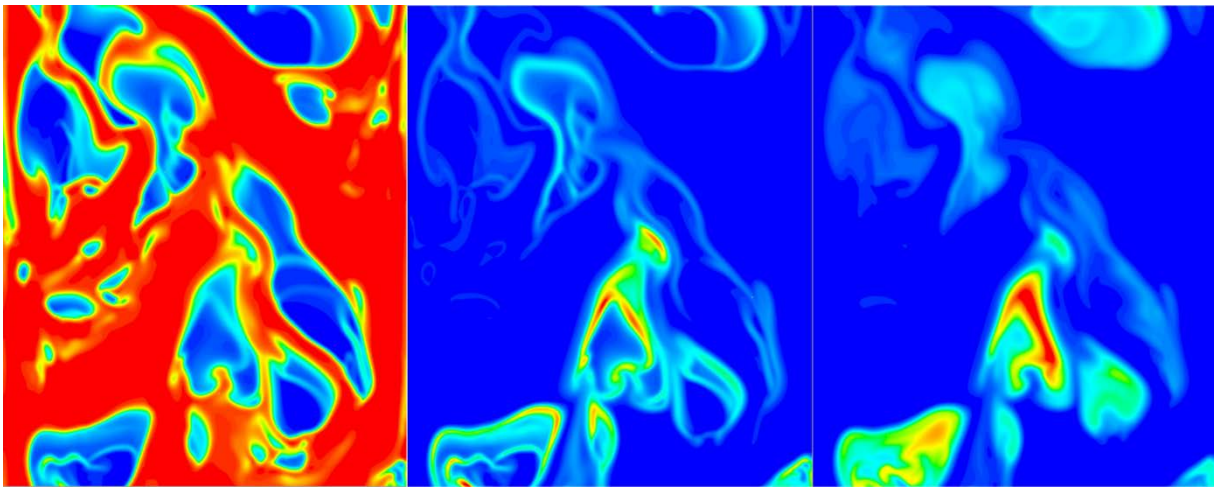

**Figure 14: Instantaneous contours of particle volume fraction (left), heterogeneous reaction rate [kmol/(m$^3$s)] (middle) and reactant mole fraction (right) extracted from the 200 µm case with 226 width-wise cells. The ranges in the three cases is from 0-0.63, 0-0.02 and 0-0.5 respectively.**

However, the importance of the resolution of the interface will depend on the permeability of the cluster. If the cluster is highly permeable (such as with large particles), gas can easily penetrate and react with solids inside the cluster (i.e. not only on the gas/solids interface). On the other hand, if the gas cannot effectively penetrate the cluster (as is the case with small particles), the majority of the reaction has to occur on the gas/solids interface.

When looking at grid independence behaviour therefore, it is reasoned that the cluster permeability is the controlling factor and, since clusters are close to maximum packing, the drag at maximum packing should be used to achieve a correlation with the grid independent cell size. This appears to be the case as shown in Figure 13.

## 5.3 Implications on large scale simulations

The very large effect of particle size on grid independence behaviour (and therefore also on simulation time) will be investigated in this section to determine the implications of this large dependency on large scale fluidized bed simulations. First of all, current computational capacities need to be quantified. From experience, the amount of points in time and space that can be computed within a reasonable timeframe using current computational capacities is roughly 3 billion. This value will of course vary greatly depending on whether only a single simulation is required for process understanding or whether tens of simulations are required for design and optimization purposes, but the aforementioned value of 3 billion is seen as a representative average. A representative example would be 30,000 timesteps of 0.001 s each (30 s of flow time in total) solved on a grid of 100,000 cells. This simulation will take about 2 days to complete on 4 cores.

If it is assumed that the industrial reactor of interest is 5 m in diameter and requires fine meshing up to a height of 10 m with a gas feed velocity of 0.5 m/s, an estimation of the particle size that can be simulated both in 2D and 3D can be made. It is further assumed that a sufficiently small,

constant timestep size is given as $\Delta t = \Delta/(20U) = \Delta/10$. This formula operates on the assumption that transient velocity spikes will not go higher than 20 times the fluidization velocity in order to keep the Courant number below 1 and was successfully used in this study. Furthermore, the assumption is made that the gas needs to pass through the bed 20 times at the given superficial velocity during the simulation in order to first achieve pseudo steady state behaviour and subsequently allow for meaningful time-averaging. For this particular industrial reactor, a simulation time of $20 \times 10 / 0.5 = 400$ seconds will be required.

As an example, a 2D mesh composed of 1 cm cells will require $(5 \times 10)/0.01^2 = 500000$ cells in this reactor, as well as $400/(0.01/10) = 400000$ timesteps. The number of points to be solved in space and time therefore amount to 200 billion, almost two orders of magnitude greater than that which is presently affordable (3 billion). Using 1 cm cells in industrial reactors is therefore still far out of reach, even in 2D.

In order to get a meaningful indication of the potentials of the fully resolved method in industrial applications, the aforementioned calculations can be completed in reverse to find the minimum cell size that could be afforded to simulate this reactor in 2D at present to be 4.05 cm. According to the data reported in Figure 4, this would permit a particle size of 667 μm to be simulated with reasonable numerical accuracy.

A further interesting study would be to project the decrease in particle size that would be possible to simulate in coming years if Moore's law of a doubling in computational capacity every two years holds firm. These results are given in Figure 15.

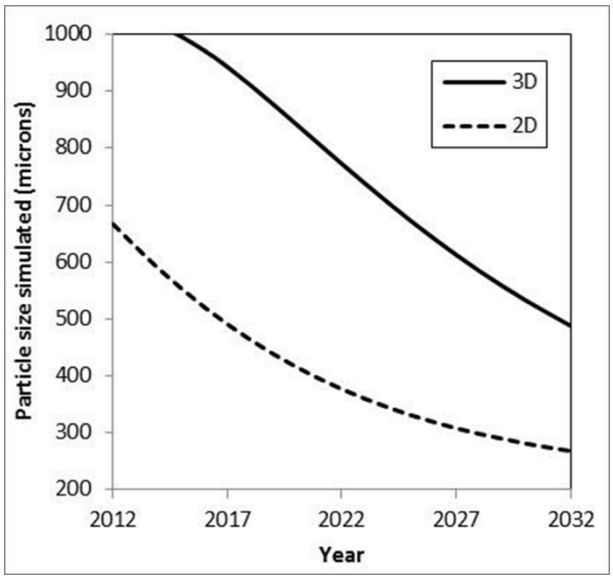


**Figure 15: Projections of the minimum particle size that would be affordable to simulate in a 5 m inner diameter industrial reactor with the TFM.**

It is clear that some useful 2D industrial work can already be done with current computational capacities for larger particles. 2D simulations are fundamentally limited and introduce a degree of uncertainty, but have been shown to give qualitatively similar process behaviour as 3D simulations [16]. 3D industrial simulations for large particle classes will also become feasible within the coming decade.

For the time being, however, it can be helpful to get an indication of the particle size that can be accurately simulated in a given reactor size. This can be attained in a similar way as above, only this time setting the reactor diameter as the independent variable and specifying its height by an expanded bed aspect ratio of 2. Using current computational facilities (the 3 billion points in time and space specified above), the correlation between reactor size and minimum particle size is given in Figure 16.

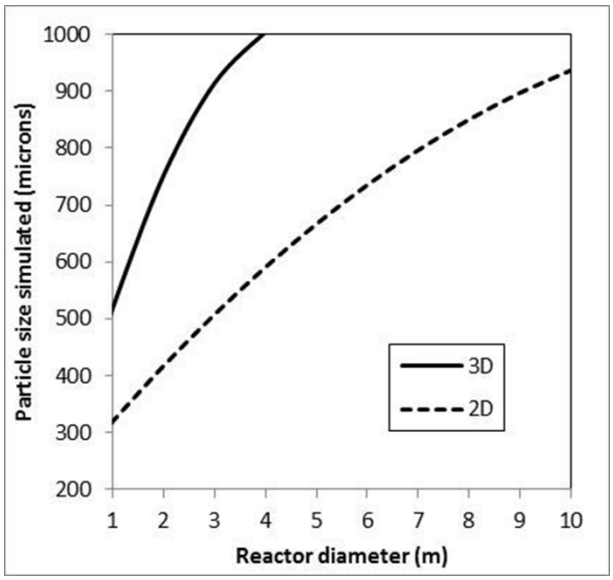


**Figure 16: Estimation of the minimum particle size that would be affordable to simulate in a reactor with a given diameter using the TFM.**

It is clear from Figure 16 that a lot of good work can be done using present models in smaller reactors. Even simulations of a 1 m reactor can be of value to industry in some cases and such a reactor can be simulated accurately with 320 µm particles in 2D and 520 µm particles in 3D. Interestingly, it has also been shown that larger particle sizes improve reactor performance when porous particles are used where the reaction occurs throughout the particle and not only on the particle surface [16]. Such reactor systems, such as Chemical Looping Combustion systems, can be evaluated numerically already today using the well-established TFM approach, thereby greatly accelerating the development of these processes.

# 6 Summary and Conclusions

Grid dependence behaviour of fluidized bed reactor simulations carried out with the standard TFM approach is greatly influenced by the particle size used in the reactor. For example, the cell size needed to achieve sufficiently grid independent results for 200 µm particles was found to be 63 times smaller than the cell size needed for sufficiently grid independent results for 1000 µm particles. The conventional wisdom of taking the cell size to be proportional to the particle size was therefore proven to be greatly in error with grid requirements becoming rapidly

less stringent as the particle size is increased. These results suggest that, if larger particles are used, industrially interesting reactor sizes can be safely simulated with models and computational resources available today. Some guidelines were given as to the particle size that can be simulated in various reactor sizes using current computational facilities. Projections were also given as to how this minimum particle size would reduce as computational power and availability increases in coming years.

Closer studies into the mechanisms behind the grid independence behaviour found that the cell size required for hydrodynamic grid independence was directly proportional to the particle relaxation time at a volume fraction of 0.3. This could be explained by noting that smaller particles have shorter relaxation times and are therefore more closely coupled to the carrier phase. Such a close coupling would require very large amounts of streamline curvature to allow particles to depart sufficiently from the gas streamlines to collide and form clusters. If the grid is not sufficiently fine to resolve such high streamline curvature, particles cannot depart from streamlines, collide and form clusters, and the physics of the system is no longer properly resolved.

For reactor performance (degree of conversion) grid independence, it was found that the grid independent cell size was proportional to the particle relaxation time at maximum packing. This could be understood by noting that the reactor performance would be primarily controlled by the ease with which the reactant gas can penetrate the dense clusters. For large particles, the cluster is highly permeable and reactant gas can easily penetrate to react throughout the cluster. For small particles, on the other hand, the cluster has a very low permeability and the reaction therefore occurs mostly on the cluster surface, thereby creating very large gradients in species concentration which require very small cells to resolve accurately.

# 7 Further work

This work will be extended to further quantify the grid independence behaviour of the TFM under bubbling fluidization by carrying out simulations at varying particle densities, gas flow rates, gas densities, gas viscosities and reaction rates. This study will properly evaluate the generality with which the particle relaxation time can be used to predict the grid independent cell size. In addition, the reliability with which the particle relaxation time can predict sufficiently grid independent cell sizes will also be assessed using different drag laws and other KTGF closures.

# 8 Acknowledgements

The authors would like to express their gratitude for the financial support from the Research Council of Norway under the Flow@CLC grant (project number: 197580). The authors also acknowledge the use of the supercomputing facilities at the Norwegian University of Science and Technology for the most expensive simulations carried out in this study.

# 9 References

[1] S. Cloete, S. Amini, S.T. Johansen, On the effect of cluster resolution in riser flows on momentum and reaction kinetic interaction, Powder Technology, 210 (2011) 6-17.
[2] D. Gidaspow, R. Bezburuah, J. Ding, Hydrodynamics of Circulating Fluidized Beds, Kinetic Theory Approach, 7th Engineering Foundation Conference on Fluidization 1992, pp. 75-82.
[3] C.K.K. Lun, S.B. Savage, D.J. Jeffrey, N. Chepurniy, Kinetic Theories for Granular Flow: Inelastic Particles in Couette Flow and Slightly Inelastic Particles in a General Flow Field, Journal of Fluid Mechanics, 140 (1984) 223-256.
[4] M. Syamlal, W. Rogers, T.J. O'Brien, MFIX Documentation: Volume 1, Theory Guide., National Technical Information Service, Springfield, 1993.
[5] F. Taghipour, N. Ellis, C. Wong, Experimental and computational study of gas-solid fluidized bed hydrodynamics, Chemical Engineering Science, 60 (2005) 6857-6867.
[6] N. Ellis, M. Xu, C.J. Lim, S. Cloete, S. Amini, Effect of Change in Fluidizing Gas on Riser Hydrodynamics and Evaluation of Scaling Laws, Industrial & Engineering Chemistry Research, 50 (2011) 4697-4706.
[7] S. Cloete, S. Amini, S.T. Johansen, A fine resolution parametric study on the numerical simulation of gas-solid flows in a periodic riser section, Powder Technology, 205 (2011) 103-111.
[8] W. Wang, J. Li, Simulation of gas-solid two-phase flow by a multi-scale CFD approach-of the EMMS model to the sub-grid level, Chemical Engineering Science, 62 (2007) 208-231.

[9] J. Wang, W. Ge, J. Li, Eulerian simulation of heterogeneous gas-solid flows in CFB risers: EMMS-based sub-grid scale model with a revised cluster description, Chemical Engineering Science, 63 (2008) 1553-1571.
[10] A.T. Andrews, P.N. Loezos, S. Sundaresan, Coarse-grid simulation of gas-particle flows in vertical risers, Industrial and Engineering Chemistry Research, 44 (2005) 6022-6037.
[11] S. Benyahia, On the effect of subgrid drag closures, Industrial and Engineering Chemistry Research, 49 (2010) 5122-5131.
[12] S. Cloete, S.T. Johansen, S. Amini, Evaluation of a filtered model for the simulation of large scale bubbling and turbulent fluidized beds, Powder Technology, 235 (2013) 91-102.
[13] W. Holloway, S. Sundaresan, Filtered models for reacting gas–particle flows, Chemical Engineering Science, 82 (2012) 132-143.
[14] S. Cloete, A. Zaabout, S.T. Johansen, M. van Sint Annaland, F. Gallucci, S. Amini, The generality of the standard 2D TFM approach in predicting bubbling fluidized bed hydrodynamics, Powder Technology, 235 (2013) 735-746.
[15] S. Cloete, S. Amini, Design strategy for a Chemical Looping Combustion system using process simulation and Computational Fluid Dynamics, Progress in Computational Fluid Dynamics, 12 (2012) 80-91.
[16] S. Cloete, S.T. Johansen, S. Amini, Investigation into the effect of simulating a 3D cylindrical fluidized bed reactor on a 2D plane, Powder Technology, 239 (2013) 21-35.
[17] S. Cloete, S.T. Johansen, S. Amini, An assessment of the ability of computational fluid dynamic models to predict reactive gas–solid flows in a fluidized bed, Powder Technology, 215-216 (2012) 15-25.
[18] B.G.M. Van Wachem, J.C. Schouten, C.M. Van den Bleek, R. Krishna, J.L. Sinclair, Comparative analysis of CFD models of dense gas-solid systems, AIChE Journal, 47 (2001) 1035-1051.
[19] D.G. Schaeffer, Instability in the Evolution Equations Describing Incompressible Granular Flow, Journal of Differential Equations, 66 (1987) 19-50.
[20] S. Ogawa, A. Unemura, N. Oshima, On the Equation of Fully Fluidized Granular Materials, Journal of Applied Mathematics and Physics, 31 (1980) 483.
[21] O. Levenspiel, Chemical Reaction Engineering, 3rd ed., John Wiley & Sons, United States, 1999.
[22] P.C. Johnson, R. Jackson, Frictional-Collisional Constitutive Relations for Granular Materials, with Application to Plane Shearing, Journal of Fluid Mechanics, 176 (1987) 67-93.
[23] H.T. Bi, J.R. Grace, Flow regime diagrams for gas-solid fluidization and upward transport, International Journal of Multiphase Flow, 21 (1995) 1229-1236.
[24] FLUENT, ANSYS FLUENT Theory Guide, ANSYS, Inc., Southpointe, 2011.
[25] S. Patankar, Numerical Heat Transfer and Fluid Flow, Hemisphere Publishing Corporation, United States, 1980.
[26] B.P. Leonard, S. Mokhtari, ULTRA-SHARP Nonoscillatory Convection Schemes for High-Speed Steady Multidimensional Flow, NASA TM 1-2568 (ICOMP-90-12)NASA Lewis Research Center, 1990.
[27] T. Li, A. Gel, S. Pannala, M. Shahnam, M. Syamlal, Reprint of “CFD simulations of circulating fluidized bed risers, part I: Grid study”, Powder Technology.